A New One-Dimensional Numerical model for Unsteady Hydraulics of Sediments in Rivers

Eman AlQasimi[1] MSc, Tew-Fik Mahdi[2] Ph.D.

[1] Ph.D., Dept. of Civil, Geological and Mining, Ecole Polytechnique de Montreal, C.P. 6079, Succursale Centre-Ville, Montreal, QC, Canada H3C 3A7. Email: Eman.Alqasimi@polymtl.ca

[2] Professor, Dept. of Civil, Geological and Mining, Ecole Polytechnique de Montreal, C.P. 6079, Succursale Centre-Ville, Montreal, QC, Canada H3C 3A7 (corresponding author). Email: Tewfik.Mahdi@polymtl.ca, (ORCID: https://orcid.org/0000-0003-2480-0523)

Abstract: This paper presents the model UMHYSER-1D (Unsteady Model for the HYdraulics of SEdiments in Rivers 1-D), a one-dimensional hydromorphodynamic model capable of representing water surface profiles in a single river or a multiriver network, with different flow regimes considering cohesive or non-cohesive sediment transport. It has both steady and unsteady flow and sediment modules. For steady gradually varied flows, UMHYSER-1D uses the standard step method to solve the energy equation and the "NewC" scheme for the de St Venant equations. For sediment transport, UMHYSER-1D uses two methods: for long-term simulation, the unsteady terms of the sediment transport continuity equation are ignored, and a non-equilibrium sediment transport method is used. For short-term simulation, the convection-diffusion equation, with a source term arising from sediment erosion/deposition is solved using the fractional step method. The equation without the source term is solved with an implicit finite-volume method, then the equation with source term is solved. Internal boundary conditions, such as time-stage tables, rating curves, weirs, bridges, and gates are simulated. Incorporated is the active layer concept, which allows selective erosion, enabling the simulation of bed armoring. Non-cohesive sediment transport equations and cohesive sediment physical processes are applied to calculate the sediment deposition and erosion. Finally, UMHYSER-1D empirically accounts for bed geometry adjustments by using a relationship between erosion width and flow rate, an angle of repose condition for bank stability and three minimization theories. The presented validation and application cases show UMHYSER-1D's capabilities and predicts its promising role in solving complex, real engineering cases.

Keywords: One-dimensional model; UMHYSER-1D; Fractional step method implicit finite-volume method; Unsteady sediment transport; Bed geometry adjustment; Minimization theories

1. Introduction

Numerical modeling is widely used in river engineering studies. Determining the risk zone caused by floods [1], investigations of river morphology changes [2,3], stream restoration projects and sediment deposition studies [4,5] are some examples of river engineering problems involving numerical modeling. Several numerical models were developed during the last decades, spanning from the simplest ones to more complex solvers. The less complicated ones are the one-dimensional (1D) models. Some do not consider riverbed erosion, such as FLDWAVE [6], by solving unsteady flow equations, while others are developed for mobile riverbeds such as GSTARS [7] or MHYSER [2] using the flow quasi-steadiness hypothesis. Others more complicated, were developed and still under improvement such as the one by El Kadi and Paquier [8], CONCEPTS [5], SRH-1D [9], CCHE1D [10], MIKE11 [11], HEC-RAS [12] or BASEMENT [13]. Even if two-dimensional (2D) models are gaining in popularity, the much longer computation time required for 2D models compared to 1D models, the least amount of field data required by 1D models, the stability of the 1D numerical schemes used to solve the governing equations with the gain in computational efficiency [14], make the use of 1D hydraulic models still needed in river engineering, particularly for applications with long rivers [15].

This paper presents a new 1D model, Unsteady numerical Model for HYdraulics of SEdiments in Rivers, UMHYSER-1D, developed at Polytechnique Montreal and still under improvement. Since its development, UMHYSER-1D went through different validation stages before its application in real engineering cases ([16,17,18]), however its numerical procedures were never published. The authors objectives are to create an efficient tool to solve real engineering problems and to have access to a numerical laboratory to be used to test new scientific findings. In fact, the advantage of developing a new tool resides in the accessibility to the source code which makes it easy to improve the model by adding new research ideas or testing new findings such as a new sediment transport equation.

UMHYSER-1D is a 1-D model developed to simulate flows in rivers and channels with or without movable boundaries. It can compute water surface elevations in complex channel networks. UMHYSER-1D is able to model both steady and unsteady flow conditions, cohesive and non-cohesive sediment transport, and rivers' width changes using minimization theories and riverbank retreat method. Moreover, hydraulics structures such as weirs, bridges, and gates along with other internal boundary conditions (such as time-stage tables, rating curves) are accounted for. In steady flow conditions, UMHYSER-1D is identical to MHYSER, Model for HYdraulics of SEdiments in Rivers, developed by Mahdi [2], where the continuity and energy equations are applied, when there are no changes in the flow regime, while the momentum and the continuity equations are used when there are changes from supercritical

to subcritical flows. For sediment transport, MHYSER models long-term situations and uses the non-equilibrium sediment transport method of Han [19].

UMHYSER-1D performs five groups of operations including water phase, sediment phase, stream tubes, riverbank stability analysis, and stream power minimization, respectively. The flowchart of the unsteady module of UMHYSER-1D, presented in this paper, is illustrated in Figure 1.

The remainder of this article is divided into six sections. In section two, the flow routine is presented, followed by the sediment routing, bed material mixing, and bed geometry adjustment presented in section three. Section four presents the numerical solution procedure for the water and sediment equations. Finally, in section five UMHYSER-1D is applied to an experimental test of a reservoir deposits' erosion following dam removal, followed by the conclusion.

2. Unsteady flow routing

For simple and complex channel networks, unsteady UMHYSER-1D solves the de Saint-Venant equations using appropriate boundary conditions.

2.1. Unsteady flow equations

For steady flows UMHYSER-1D solves the 1-D de St Venant equations [20]:

$$\begin{cases} B\dfrac{\partial h}{\partial t} + \dfrac{\partial Q}{\partial x} = 0 & (1a) \\ \dfrac{\partial Q}{\partial t} + \dfrac{\partial}{\partial x}\left(\alpha \dfrac{Q^2}{A}\right) + gA\dfrac{\partial Z}{\partial x} + gAS_f = 0 & (1b) \end{cases}$$

where, Q = discharge, B = storage width, A = cross-sectional area, t = time independent variable, x = spatial independent variable, g = gravity acceleration, α = velocity distribution coefficient, Z = water surface elevation, S_0 = bed slope, S_f = energy slope (= $Q|Q|/K^2$), and K = conveyance.

For river networks UMHYSER-1D uses the simultaneous solution procedures described by Chaudhry [21]. The unknowns are flow depths and flow discharges in each channel. For a river with N+1 cross-sections, there are 2(N+1) unknowns where N river reaches provide 2N equations. To have a unique solution, two boundary conditions provided by rivers' connections are required.

2.2. Boundary conditions

While the most used boundary conditions are a known discharge at the upstream boundary and a rating curve at the downstream boundary, in UMHYSER-1D the upstream boundary condition can be either a water discharge or a river stage, and the downstream boundary condition can be a river stage or a rating curve.

For a network, in addition to the upstream and downstream boundary conditions, the continuity equation is applied at each node with no storage allowed, and momentum equation is applied at each junction, imposing the same water level correction to all cross sections associated with the junction.

Hydraulic structures such as bridges, weirs and dams may exist along a river reach. At each internal structure, two unknowns are introduced: discharge and water surface elevation. The continuity equation along with an extra equation depending on the particular structure provides the set of equations to solve for the unknowns. UMHYSER-1D supports 4 types of internal boundary conditions. A stage time series represents a controlled pool or lake and a rating curve represents any structure having a unique relationship between flow rate and water surface elevation. Moreover, weirs and bridges are implemented in the same way as done in [12] and [6] respectively.

3. Sediment routing

After the water surface characteristics are calculated, the cross sections are divided into sections of equal conveyance or stream tubes (Figure 2).

These stream tubes act as conventional 1-D channels with known hydraulic properties where sediment routing can be carried out within each stream tube almost as if they were independent channels. Once the top widths are determined, the velocities of the stream tubes are calculated by giving a crosswise velocity distribution. Stream tube locations can vary with time. Therefore, although no material can cross stream tube boundaries during a time step, lateral movement of sediment is described by lateral variations in the stream tube boundaries. For a short-term simulation, the governing equation for sediment transport is a convection-diffusion equation with a source term arising from sediment erosion/deposition.

3.1. Total load convection-diffusion equation

In the present paper, the 1-D version of the 2-D unsteady total load convection-diffusion equation to model depth-averaged non cohesive sediment transport, developed in [22], automatically switches to suspended load, bed load, or mixed load depending on a transport mode parameter consisting of local flow hydraulics. Moreover, this equation can be applied to multiple size fractions and is generalized to cohesive sediment transport.

The 1-D version of Greimann et al. equation [22], cross-sectional averaged convection-diffusion equation is:

$$\frac{\partial AC}{\partial t} + \frac{\partial \beta QC}{\partial x} = \frac{\partial}{\partial x}\left(AfD\frac{\partial C}{\partial x}\right) + \Gamma \tag{2}$$

Where A = cross-sectional area, C = cross-sectional averaged sediment concentration by volume, Q = flow rate, D= longitudinal diffusion coefficient, Γ = source term, x = longitudinal distance and t = time.

To provide model closure, three variables still need to be determined: the transport mode parameter f, the velocity ratio β, and the source term Γ. The f parameter represents the ratio of suspended portion to the total sediment concentration for a single size class; it ranges from 0 for pure bed load to 1 for pure suspended load, while β is the ratio of sediment velocity to flow velocity. Two expressions for β are needed, one for bed load, β_{bed}, and the other for suspension case, β_{sus}. The following expressions for f and β are given in [19]:

$$f = \min\left(1, 2.5e^{-z}\right) \tag{3}$$

$$\beta_{bed} = \frac{u_*}{V_t}\frac{1.1\emptyset^{0.17}\left(1-e^{-5\emptyset}\right)}{\sqrt{\theta_r}} \tag{4a}$$

$$\beta_{sus} = 1 + \frac{u_*}{2\kappa V_t}\left(1 - e^{2.7z}\right) \tag{4b}$$

$$\beta = \max\left(\beta_{bed}, \beta_{sus}\right) \tag{5}$$

where $z = \omega_f/(\kappa u_*)$ is the suspension parameter, and $\emptyset = \theta/\theta_r$, $\theta = \tau_b/[\gamma(s-1)d]$ = Shields parameter (τ_b = bed-shear stress; γ = specific weight of water; d = particle diameter; and s = specific gravity of sediment); and θ_r = reference non-dimensional shear stress, the Shields parameter at which there is a low but measurable reference transport rate, such as defined in [23].

Note that z must be less than 1 when computing β_{sus}, and $\emptyset$ must be less than 20 when computing β_{bed}[19]. Further, Equation (5), permitting the use of the same Equation (2) for simulating bed load and suspended load, avoids the discontinuity in sediment velocity between bed load and suspended load, using equations. (4a) and (4b). In addition, the longitudinal diffusion coefficient, D, is computed as in [24]:

$$D = K\frac{W^2U^2}{Hu_*} \tag{6}$$

where W = channel top width, U = cross sectional velocity, H = average cross-sectional depth, u_*= shear velocity, and K = user specified value ([24] recommend 0.011).

Source term Γ

<u>Non cohesive sediment</u>

For non-cohesive sediment the following source term is used [25,26]:

$$\Gamma = \frac{1}{L_{tot}}\left(q^*_{tot} - q_{tot}\right)W \tag{7}$$

where L_{tot}= total effective adaptation length, W= channel top width, q^*_{tot}= equilibrium capacity for total load transport rate (per unit width), and q_{tot}= actual total load transport rate (per unit width).

UMHYSER-1D offers a choice of 12 equilibrium capacity equations [23, 27-38], widely used in river engineering. Using the sediment recovery factor, α, related to L_{tot} [22]:

$$L_{tot} = (1-f)L_b + f\frac{Uh}{\alpha\omega_s} \tag{8a}$$

where $L_b = b_L h$ = adaptation length for bed load, b_L= a calibration coefficient, h= water depth.

L_{tot} might be calculated as [39]

$$L_{tot} = \max(L_b, L_s) \tag{8b}$$

with $L_s = \frac{Uh}{\alpha\omega_s}$= adaptation length for suspended load. If bed load and suspended load coexist, L_b is generally smaller than L_s and $L_{tot} = L_s$; in fact, L_b is set to one or two times the grid spacing [40]. But since L_b and L_s (i.e., α) are used as calibration parameters, the difference between and is negligible.

For suspended load (f=1), from Eq.(8a):

$$\alpha = \frac{Uh}{L_{tot}\omega_s} \tag{8c}$$

where ω_s = suspended particle fall velocity, equation (7) takes the form:

$$\Gamma = \alpha\omega_s(C^* - C)W \tag{9a}$$

or

$$\Gamma = (V_E - V_D C)W \tag{9b}$$

where C^*= cross-section averaged sediment concentration capacity by volume and C= cross-section averaged sediment concentration by volume, $V_E = \alpha\omega_s C^*$, and $V_D = \alpha\omega_s$.

In the case of multiple size fractions, equation (9b) is valid for each material of size k:

$$\Gamma_k = \left(V_{E,k}p_k - V_{D,k}C_k\right)W \tag{10}$$

where p= percentage of material of size k, C_k= cross-section averaged sediment concentration by volume for material of size k, $V_{E,k}$= $\alpha\omega_{s,k}C^*_k$, $V_{D,k}$= $\alpha\omega_{s,k}$, $\omega_{s,k}$= fall velocity for particle of size class k, and C^*_k= sediment concentration capacity by volume computed if the bed was composed entirely of this k size fraction ($C_{*k} = p_k C^*_k$, sediment concentration capacity by volume of size class k).

The complexity of the sediment recovery factor, α, is well discussed in [39]. Suggested values for α are about 0.25 for strong deposition, and 1 for strong erosion [19,41]. In UMHYSER-1D, $b_L$and α are user defined calibration parameters and different values of α are used for deposition versus erosion.

Cohesive sediment

Treated as a single sediment class, cohesive sediment is still modeled by equation (2) but the expression of the source term, Γ, is given by:

$$\Gamma = (V_E p_c - V_D C_c)W \tag{11}$$

where V_E and V_D are the velocities of erosion and deposition, respectively, p_c is the percentage of the cohesive sediment in the riverbed, and C_c is the cross-section averaged cohesive sediment concentration by volume. UMHYSER-1D deposition of cohesive sediment is based on Krone's equation [42], while particle and mass erosion are based on the work of Parthenaides [43] and adapted by Ariathurai and Krone [44]. V_E is defined by:

$$V_E = \begin{cases} 0 & if \quad \tau \leq \tau_{es} & (12a) \\ \dfrac{P_s}{\rho_s}\left(\dfrac{\tau - \tau_{es}}{\tau_{em} - \tau_{es}}\right) & if \quad \tau_{es} \leq \tau \leq \tau_{em} & (12b) \\ \dfrac{P_s}{\rho_s} + \dfrac{P_m}{\rho_s}\left(\dfrac{\tau - \tau_{em}}{\tau_{em}}\right) & if \quad \tau_{em} \leq \tau & (12c) \end{cases}$$

P_s = surface erosion constant (kg/m²/s), P_m = mass erosion constant (kg/m²/s), τ = bed shear stress (Pa), ρ_s = sediment density (kg/m³), τ_{es}= critical surface erosion shear stress (Pa), τ_{em}= critical mass erosion shear stress (Pa). The deposition velocity, V_D, is given by:

$$V_D = \begin{cases} \left(1 - \dfrac{\tau}{\tau_{df}}\right)\omega & if \quad \tau \leq \tau_{df} & (13a) \\ \left(1 - \dfrac{\tau}{\tau_{dp}}\right)\omega\left(1 - \dfrac{C_{eq}}{C_c}\right) & if \quad \tau_{df} \leq \tau \leq \tau_{dp} \ and \ C_{eq} \leq C_c & (13b) \\ 0 & if \quad \tau_{dp} \leq \tau \ \ or \ \ C_{eq} \geq C_c & (13c) \end{cases}$$

C_c = cross-section averaged sediment concentration by volume, τ = bed shear stress (Pa), C_{eq}= equilibrium cohesive cross-section averaged sediment concentration by volume, τ_{df}= critical shear stress for full deposition (Pa), ω = fall velocity of the cohesive sediment (m/s), and τ_{dp}= critical shear stress for partial deposition (Pa).

3.2. Fall velocity

For sediment fall velocity, UMHYSER-1D adopts the approach of the US Bureau of Reclamation [9, 45] for both cohesive and non-cohesive sediments. More specifically, for non-cohesive sediment recommended values of [46] for particle diameter less than 10 mm are adopted. For particle's diameter higher than 10 mm, the following formula is used [45]:

$$\omega = 1.1\sqrt{(s-1)gd} \tag{14a}$$

where ω is the fall velocity, g = acceleration due to gravity, s = specific gravity of sediments, and d = particle diameter.

For particles in the silt and clay size ranges, that is, with diameters between 1 and 62.5 μm, the unhindered sediment fall velocity is computed from [45]:

$$\omega = \frac{(s-1)gd^2}{18\nu} \tag{14b}$$

Where ν = kinematic viscosity of water. This equation is valid for a user defined value of the concentration, C_1.

In fact, the fall velocity for cohesive sediments depends on the concentration. UMHYSER-1D defines cohesive fall velocity according to figure 3 [9], where the user defined a set of site specific 4 points data (C_1, ω_1, C_2, ω_2, C_3, ω_3, C_4, ω_4).

3.3. Bed material mixing

UMHYSER-1D uses the method of Bennett and Nordin [47] for the bed composition accounting procedure by dividing the bed into conceptual layers. The top layer, or active layer contains the bed material available for transport, beneath which is the storage layer or inactive layer, and finally the undisturbed bed. The active layer is the most important layer in this procedure. Erosion of a particular size class of bed material is limited by the amount of sediment of this size class present in the active layer. If the flow carrying capacity for a particular size class is greater than what is available for transport in the active layer, the term availability limited is used [47]. On the other hand, if more material is available than the computed carrying capacity by a sediment transport equation, the term capacity limited is used. At the end of each time step, bed material is calculated in each stream tube. At the beginning of the next time step, after the new locations of the stream tube boundaries are determined, these values are used to compute the new layer thickness and bed composition. Figure 4 illustrates this procedure.

3.4. Bed geometry updating and adjustments

By solving mass conservation equation, (15), the average depth of erosion/deposition is obtained for each size class:

$$(1 - n_k)W\frac{\partial z_{b,k}}{\partial t} = -\Gamma_k \tag{15}$$

where n_k= porosity for the k-th size class in the active layer, and $\frac{\partial z_{b,k}}{\partial t}$ = change in the bed elevation, z_b, due to sediment class k. The source term, Γ_k, is given by equation (10) and (11) for non-cohesive and cohesive sediment respectively. The total depth of deposition/erosion in a cross-section, Δz_b, is the sum of all the bed changes of the different size classes, $\Delta z_{b,k}$.

The erosion width is an important parameter in estimating the erosion details. Because 1-D models do not have a shear stress that varies across a cross-section, it is difficult to estimate the non-uniform erosion that occurs during incision. Since UMHYSER-1D is a 1-D model, it does not directly simulate lateral transport of sediment; however it empirically accounts for the processes involved by using a relationship between erosion width and flow rate, and an angle of repose condition for bank stability. The erosion width, centered at the centroid of the cross section is given by:

$$Wer = aQ^b \tag{16}$$

where Wer = erosion width, Q = stream flow, and a and b are user defined constants.

During erosion progression, the steepness of bank slope is limited by the above and under water values of the angle of repose. At the end of each time step, if vertical or horizontal adjustments have caused the bank to become too steep, the two points adjacent to the segments of the banks are adjusted vertically until the slopes equal the critical slopes. The material taken from the banks will be added during the next time step as a lateral sediment discharge.

Moreover, as an option UMHYSER-1D offers the choice of 3 minimization theories for the determination of depth and width adjustments, at a given time step: minimization of the total stream power [48], minimization of the energy slope [49] and minimization of the bed slope (or conveyance maximization).

According to the minimization of total stream power theory, if lower total stream power is the result of alteration of the channel widths, then channel adjustments are made in the lateral direction. Otherwise, the adjustments progress in the vertical direction.

While adopting the minimization of energy slope, if the energy slope at a cross-section is greater than the weighted average energy slope of its adjacent sections, then the channel width at this section is reduced during deposition or the depth is increased during erosion. However, if the energy slope is smaller the channel depth at this section is decreased during deposition or an increase of width occurs during erosion.

Finally, for the minimization of bed slope, if the bed slope at a cross-section is greater than the weighted average bed slope of its adjacent cross-sections, then the channel width at this section is reduced during deposition, or the depth is increased during erosion. Otherwise, the channel depth at this section is decreased during deposition or the width is increased during erosion.

4. Numerical solution procedure

In the case of steady flow, for backwater computations, the standard step method is used [50]. Computations proceed in the upstream direction for subcritical flows and in the downstream direction for supercritical flows. The Exner equation is then solved for bed updating [2].

For unsteady flow conditions, the set of PDEs, Equations (1a), (1b) and (2), are solved using a decoupled approach. First, for the liquid phase, the de St Venant equations are solved using the NewC numerical scheme [51], which assures numerical stability in the transition between different flow regimes, then the solid phase equation is solved using the fractional step method [52].

4.1. De St Venant equations

Equations (1a) and (1b) are solved using the NewC scheme [51] which uses a staggered grid, where the computational points for flow, Q, are located at the cross-sections, with a weighting implicit factor θ in the time dimension ($0 \leq \psi \leq 1$), and Z points are located halfway between the cross-sections (figure 5).

Application of the modified NewC scheme leads to the following set of equations:

$$a_i\, Q_{i-1}^{n+1} + b_i\, Q_i^{n+1} + c_i\, Q_{i+1}^{n+1} = d_i \tag{17a}$$

$$Z_{i+1/2}^{n+1} = \varepsilon_{i+1/2}\, Q_i^{n+1} + \beta_{i+1/2}\, Q_{i+1}^{n+1} + \gamma_{i+1/2} \tag{17b}$$

All the details are given in [46], but for completeness, the expressions of the coefficients in equations (17a) and (17b) are recalled here:

$$a_i = -\frac{\alpha\psi\Delta t}{\Delta x}\frac{Q_i^{n+\frac{1}{2}}}{A_i^{n+\frac{1}{2}}} - g\,\frac{\psi\Delta t}{\Delta x}A_i^{n+\frac{1}{2}}\varepsilon_{i-1/2}^{n+\frac{1}{2}} \tag{18a}$$

$$b_i = 1 + g\Delta t\,\frac{A_i^{n+\frac{1}{2}}}{K_i^{n+\frac{1}{2}}}|Q_i^n| + g\,\frac{\psi\Delta t}{\Delta x}A_i^{n+\frac{1}{2}}\left(\varepsilon_{i+1/2}^{n+1} - \beta_{i-1/2}^{n+1}\right) \tag{18b}$$

$$c_i = \frac{\alpha\psi\Delta t}{\Delta x}\frac{Q_i^{n+\frac{1}{2}}}{A_i^{n+\frac{1}{2}}} + g\,\frac{\psi\Delta t}{\Delta x}A_i^{n+\frac{1}{2}}\beta_{i+1/2}^{n+1} \tag{18c}$$

$$d_i = Q_i^n - gA_i^{n+\frac{1}{2}}\frac{\Delta t}{\Delta x}\left[\psi\left(\beta_{i+\frac{1}{2}}^{n+1} - \beta_{i-\frac{1}{2}}^{n+1}\right) + (1-\psi)\left(Z_{i+\frac{1}{2}}^n - Z_{i-\frac{1}{2}}^n\right)\right] + \left[-\frac{\alpha(1-\psi)\Delta t}{\Delta x}\frac{Q_i^{n+\frac{1}{2}}}{A_i^{n+\frac{1}{2}}}(Q_{i+1}^n - Q_{i-1}^n)\right] \tag{18d}$$

$$\varepsilon_{i+1/2} = -\beta_{i+\frac{1}{2}} = \frac{\psi\Delta t}{\Delta x\, B_{i+1/2}^{n+1/2}} \tag{18e}$$

$$\gamma_{i+1/2} = h_{i+1/2}^n - \frac{(1-\psi)\Delta t}{\Delta x\, B_{i+1/2}^{n+1/2}}(Q_{i+1}^n - Q_i^n) \tag{18f}$$

Written for all $i = 0, N$; the system of equations, (17a), with an upstream and a downstream boundary conditions, is solved using the double sweep algorithm [53, 54]. Then, for each i, equation (17b) provides the water surface elevations.

The numerical scheme is able to model sub-, super- and trans-critical flow conditions, but even if linearized stability analysis using Fourier series expansions [55] shows that the numerical scheme is always stable for $(0.5 < \psi \leq 1)$ [51], it has been noticed that, for Froude numbers of more than 1.5, flows start to show some wiggles that might grow into instability. As a remedy, the Local Partial Inertia [6] consisting of multiplying the acceleration term of equation (1b) by $max(0, 1 - F^n)$, where F is Froude number and n is a user specified integer, is applied. Another option consists of introducing some numerical diffusion (for example, for $\psi = 0.7$) to smooth the solution [51]. Moreover, as by its construction, the NewC scheme has some limitations in solving for supercritical flow. In fact, it requires one boundary condition at each end of the domain. Hence, supercritical flow should not occur at the upstream or downstream boundaries of any modeled river reach.

4.2. Convection-diffusion equation

The convection-diffusion, equation (2), is solved using the fractional step method [52]. Solving equation (2) is equivalent to solving the following equations:

$$\frac{\partial AC}{\partial t} + \frac{\partial \beta QC}{\partial x} = \frac{\partial}{\partial x}\left(AfD\frac{\partial C}{\partial x}\right) \tag{19a}$$

$$\frac{\partial AC}{\partial t} = \Gamma \tag{19b}$$

Equation (19a) is solved, using a finite volume method, to obtain intermediate solution, AC, then the initial value problem in (19b) is solved to obtain the solution at the next time step. This section details the solution of (19a).

Using the finite volume method, the stream is discretized into cells centred on the cross sections (figure 6), and (19a) is transformed to an integral one to conserve mass:

$$\frac{\partial}{\partial t}\int_x ACdx + \sum(\beta QC) = \sum\left(AfD\frac{\partial C}{\partial x}\right) \tag{19c}$$

<u>Unsteady term</u>

Using the explicit Euler method, the unsteady term is discretized as:

$$\frac{\partial}{\partial t}\int_x ACdx = \frac{C_P^{n+1} - C_P^n}{\Delta t} A_P \Delta x_P = a_P^u C_P^{n+1} - a_P^u C_P^n \tag{20a}$$

where n and $n+1$ = current and next time steps respectively. The subscript P indicates where the terms are approximated, at the center of the control volume, and:

$$a_P^u = \frac{A_P \Delta x_P}{\Delta t} \tag{20b}$$

Convective term

Following Pletcher et al. ([56], pp 182-184), the convective term:

$$\sum(\beta QC) = (\beta QC)_e - (\beta QC)_w \tag{21}$$

is discretized using a Lax-Wendroff TVD method:

$$(\beta QC)_e = \frac{1}{2}\{(\beta Q)_e[C_P + C_E] - Y_e[C_E - C_P]\} \tag{22}$$

with $Y_e = |(\beta Q)_e|\left[1 - \varphi\left(1 - \frac{\Delta t}{A_P \Delta x_P}|(\beta Q)_e|\right)\right]$, where $\varphi$is the flux limiter. In the literature, different limiters exist with the same performance [57]. In this paper, the limiter function of Van Leer [58] is used:

$$\varphi = \frac{r+|r|}{1+r};\ r = \begin{cases} \frac{C_E - C_P}{C_P - C_W} & if(\beta Q)_e > 0 \\ \frac{C_P - C_E}{C_E - C_{EE}} & if(\beta Q)_e < 0 \end{cases} \tag{23}$$

To get second order accuracy in time, the Crank-Nicolson method is used:

$$C \quad = \psi C^{n+1} + (1-\psi)C^n = C^n + \psi(C^{n+1} - C^n) = C^n + \psi \Delta C \tag{24}$$

where $\theta =$ implicit factor ($0 \leq \psi \leq 1$). Equation (22) takes the final form:

$$(\beta QC)_e = \frac{\psi}{2}[(\beta Q)_e + Y_e]C_P^{n+1} + \frac{(1-\psi)}{2}[(\beta Q)_e + Y_e]C_P^n + \frac{\psi}{2}[(\beta Q)_e - Y_e]C_E^{n+1} + \frac{(1-\psi)}{2}[(\beta Q)_e - Y_e]C_E^n \tag{25}$$

and the convective term, equation (21) can be written as:

$$\sum(\beta QC) = a_P^c C_P^{n+1} + a_E^c C_E^{n+1} + a_W^c C_W^{n+1} + \frac{1-\psi}{\psi}(a_P^c C_P^n + a_E^c C_E^n + +a_W^c C_W^n) \tag{26}$$

where

$$a_P^c = \frac{\psi}{2}[(\beta Q)_e + Y_e] - \frac{\psi}{2}[(\beta Q)_w - Y_w] \tag{27a}$$

$$a_E^c = \frac{\psi}{2}[(\beta Q)_e - Y_e] \tag{27b}$$

$$a_W^c = -\frac{\psi}{2}[(\beta Q)_w + Y_w] \tag{27c}$$

Diffusive term

To get a second-order accurate discretization in both space and time, the diffusive term is approximated using the central differential scheme in space [56]:

$$\sum\left(AfD\frac{\partial C}{\partial x}\right) = (Af)_e D_e \frac{C_E - C_P}{\Delta x_e} - (Af)_w D_w \frac{C_P - C_W}{\Delta x_w} \tag{28}$$

then, followed by the Crank-Nicolson method in time, using equation (22):

$$\sum\left(AfD\frac{\partial C}{\partial x}\right) = -a_P^d C_P^{n+1} - a_E^d C_E^{n+1} - a_W^d C_W^{n+1} - \frac{(1-\psi)}{\psi}[a_P^d C_P^n + a_E^d C_E^n + a_W^d C_W^n] \tag{29}$$

where:

$$a_E^d = -\psi \frac{(Af)_e D_e}{\Delta x_e} \tag{30a}$$

$$a_W^d = -\psi \frac{(Af)_w D_w}{\Delta x_w} \tag{30b}$$

$$a_P^d = -(a_E^d + a_W^d) \tag{30c}$$

Integral equation

Using equations (20a), (26) and (29), the integral equation (19c) takes the form:

$$a_P C_P^{n+1} + a_E C_E^{n+1} + a_W C_W^{n+1} = -\frac{(1-\psi)}{\psi}[a_P C_P^n + a_E C_E^n + a_W C_W^n] \tag{31}$$

where, using equations (20b), (27abc) and (30abc):

$$a_P = a_P^u + a_P^c + a_P^d \tag{32a}$$

$$a_E = a_E^c + a_E^d \tag{32b}$$

$$a_W = a_W^c + a_W^d \tag{32c}$$

The solution, C_i^{n+1} , at every cross-section *i*, is the intermediate solution to be used in equation (18b) which is solved analytically, or using Runge-Kutta 4th order method [59] to obtain the new solution $C_{i,*}^{n+1}$ at the next time step,

4.3. Bed elevation change

Finally, combining equation (19b) and mass conservation, equation (15), the average depth of deposition/erosion for each size fraction *k*, at a cross section *i*, is calculated as:

$$\Delta z_{b,k} = -\frac{(C_{i,*}^{n+1} - C_i^{n+1})A_i}{(1-n_k)W} \tag{33}$$

where: $\Delta z_{b,k}$= bed elevation change due to sediment class *k,* n_k= porosity for the k-th size class in the active layer, A_i = Cross-sectional area and W = channel top width.

The sediment transport is computed for each individual sediment size fraction within each stream tube then the total bed changes, Δz_b, are computed as a sum of the bed changes due to each particle size, $\Delta z_{b,k}$.

Even if the NewC scheme is unconditionally stable for $0.5 < \psi \leq 1$, to ensure the validity of the uncoupled approach used by UMHYSER-1D, numerical experimentation is required to determine a suitable time step to be used.

5. Application

This section presents the results of UMHYSER-1D applied to an experimental test case to show its capabilities and limitations.

Experiment

Cantelli et al. [60] performed experiments, of 1.5 hours duration, at the University of Minnesota to simulate dam removal. A flume of a width of 0.61 m and a slope of 0.018 was filled with uniform coarse sand, of d_{50} = 0.8 mm, to replicate the sediment deposit behind a dam. The maximum depth of the sediment layer is 0.12 m. To ensure that the erosion occurred in the middle of the flume, a channel 1 cm deep and 27.5 cm wide was cut in the middle of the deposit. Constant water flow rate of 0.3 l/s and sediment rate of 0.002 kg/s ensure an equilibrium supply rate at the given slope and width. During bed erosion, precise measurement of the bed profile of the dam were done, but there were no cross-sectional data available to compare the results. Because the vertical erosion in the middle of the channel was faster than the additional sediment supply from the banks, Cantelli et al. [60] observed a rapid narrowing of the channel followed by a gradual widening.

Model inputs

In UMHYSER-1D, the points representing each cross-section are spaced 1 cm and the cross-sections are spaced 10 cm apart. Several simulations were performed to achieve the ''best'' one. For the base case simulation, Manning's roughness coefficient is assumed equal to 0.025, Parker sediment transport capacity equation is used, and the angles of repose used for bank failure modeling are set to 70 degrees for the angle of repose above water, and to 45 degrees for the angle of repose below water. Moreover, the erosional width is assumed to be 24 cm, and the default value of the non-dimensional critical shear stress needed to use Parker's equation is used (θc = 0.0386) along with the adaptation length for bed load, $L_b = 10\ cm$. Table 1 summarizes the main input data for the base case and for the 23 simulations performed by changing one parameter at a time.

Model Results:

To find the best data set that gave the best results (closest simulated longitudinal profile to the observed one), sensitivity analysis is performed. Figures 7 to 14 show the effects of sediment transport capacity equation, angles of repose, erosional width, non-dimensional critical shear stress, minimization theories, adaptation length for bed load, diffusive wave approximation, and Manning coefficient respectively. The observed final longitudinal profile is compared to the simulated ones at time 1.5 hours.

The Manning coefficient of 0.025 offers better results while Parker's bedload transport equation, developed for gravel bed sediment, presents the best results even if the sediments in this experiment is coarse sand. It is not surprising that Parker's [23] equation performs well since the used sediments were transported mainly in bedload

mode. The non-dimensional critical shear stress needed to use Parker's equation was assigned a value of $\theta_c = 0.03$. Note that the value of hiding factor, α, is not important because only a single size class is being simulated. The angles of repose used for bank failure modeling are set to 70 degrees for the angle of repose above water, and to 30 degrees for the angle of repose below water. The adaptation length for bed load non-equilibrium sediment transport have little impact on bed evolution. This is mainly because the max water depth (less than 1 cm) is smaller than the distance between two cross-sections (10 cm). In this experiment, equilibrium sediment transport prevailed. Finally, erosional width is used to empirically accounts, via Eq. (16), for the observed rapid narrowing of the channel followed by a gradual widening. Better results are achieved using an erosional width of 30 cm. If the minimization of bed slope and energy slope show practically no improvement over the initial simulation, the minimization of total stream power improved significantly the bed profile at the knickpoint. Finally, the diffusive wave equation approximation produces better results than the full dynamic wave equation by smoothing the bed waves at the knickpoint.

Figure 15 shows the results of the best simulation for the best input data corresponding to simulation Sim 21. The simulated results are compared to the experiment results of Run 6 of [60]. Overall, the agreement between the measured and simulated longitudinal profiles is very satisfactory. For cross-sections changes, Figure 16 shows the example of the cross-section corresponding to the knickpoint. Note that there were no cross-sectional data to compare the model against, but Cantelli et al. [60] observed a rapid narrowing of the channel followed by a gradual widening. UMHYSER-1D cannot model the observed cross-section evolution since it does not directly simulate lateral transport of sediments. In fact, it cannot model the rapid narrowing of the channel followed by a gradual widening.

6. Conclusion

This paper presents UMHYSER-1D, a newly developed 1-D hydromorphodynamic model. It handles subcritical and supercritical regimes and cohesive and non-cohesive sediments. Moreover, UMHYSER-1D allows modeling of a single natural channel or multichannel looped networks with different types of internal boundaries and hydraulics structures.

In steady flow conditions, UMHYSER-1D is identical to MHYSER, (Mahdi, 2009). Under unsteady flow conditions, UMHYSER-1D uses a decoupled approach: First, the "NewC" scheme is used to solve the de St Venant equations, then the total load convection-diffusion equation is solved using the fractional step method. The equation without the source term is solved with an implicit finite-volume method, then the equation with source term is

solved to obtain the sediment concentration at the next time step. The active layer, concept and sediment physical processes are applied to calculate the sediment deposition and erosion. Finally, UMHYSER-1D empirically accounts for bed geometry adjustments by using a relationship between erosion width and flow rate, an angle of repose condition for bank stability and three minimization theories.

An experimental erosion test is used to test the capabilities of UMHYSER-1D to predict the erosion of reservoir deposits following dam removal. Since UMHYSER-1D is a 1D model, it cannot model satisfactory transversal cross-sectional evolution, but sensitivity analysis allowed the identification of the best input data set that reproduced very satisfactory the longitudinal profile evolution. Hence, even at small scale (laboratory flumes), UMHYSER-1D performs very well. For this case, no observed cross-sectional data were available. This is an important issue because the greatest uncertainty in applying 1D model reside in the estimation of the streamwise sediment transport.

Finally, the previous applications of UMHYSER-1D and the present experimental test case show the capabilities of this model and predicts its promising role in solving complex real engineering cases and its use as a numerical laboratory to test available or new scientific findings.

Acknowledgement

This research was supported in part by a National Science and Engineering Research Council (NSERC) Discovery Grant, application No: RGPIN-2016-06413.

Conflicts of interest/Competing interests: On behalf of all authors, the corresponding author states that there is no conflict of interest.

References

1. Mahdi T (2007). Pairing Geotechnics and Fluvial Hydraulics for the Prediction of the Hazard Zones of an Exceptional Flooding. Natural Hazards, 42(1):225-236
2. Mahdi T (2009). Semi-Two-Dimensional Numerical Model for River Morphological Change Prediction: Theory and Concepts. Natural Hazards, 49(3): 565-603
3. Formann E, Habersack HM, Schober S (2007). Morphodynamic river processes and techniques for assessment of channel evolution in Alpine gravel bed rivers. Geomorphology, 90(3-4): 340-355
4. Lauer WJ, Parker G (2008). Modeling framework for sediment deposition, storage, and evacuation in the floodplain of a meandering river: Application to the Clark Fork River, Montana. Water Res. Research. 44(8)

5. Langendoen EJ (2000). CONCEPTS - CONservational Channel Evolution and Pollutant Transport System Report, U.S. Department of Agriculture, Agricultural Research Service, National Sedimentation Laboratory, Oxford, MS
6. Fread DL, Lewis JM (1998). NWS FLDWAV Model, Hydrologic Research Laboratory, Office of Hydrology, National Weather Service (NWS), NOAA, Silver Spring, MD
7. Yang CT, Simoes FJM (2002). User's Manual for GSTARS 3.0 (Generalized Stream Tube model for Alluvial River Simulation version 3.0). U.S. Bureau of Reclamation, Technical Service Center, Denver, CO
8. El kadi Abderrezzak, K, Paquier A (2009). One-dimensional numerical modeling of sediment transport and bed deformation in open channels, Water Resour. Res., 45, W05404
9. Greimann B, Huang JV (2018). SRH-1D 4.0 User's Manual (Sedimentation and River Hydraulics – One Dimension, Version 4.0). Technical Report SRH-2018-07, Technical Service Center, US Bureau of Reclamation, Denver (CO), USA
10. Vieira DA, Wu W (2002). One-dimensional channel network model CCHE1D version 3.0 - User's Manual, report, Natl. Cent. for Comput. Hydrosci. and Eng., Univ. of Mississipi, Oxford, Miss.
11. DHI (2009). MIKE 11: A modeling system for rivers and channels. Reference manual. Danish Hydraulic Institute, Denmark
12. Brunner GW (2016). HEC-RAS River Analysis System Hydraulic Reference Manual. US Army Corps of Engineers; Report No. CPD-69. Hydrologic Engineering Center (HEC), Davis, CA, USA
13. Vetsch D, Rousselot P, Volz C, Vonwiller L, Peter S, Ehrbar D, Mueller R (2017). System Manuals of BASEMENT, Version 2.7. Laboratory of Hydraulics, Glaciology and Hydrology, ETH Zurich
14. Papanicolaou A N, Elhakeem M, Krallis G, Prakash S, Edinger J (2008). Sediment transport modeling review-current and future developments. J. Hydraulic Engineering. 134:1-14
15. Deal EC (2016). A Comparison Study of One- and Two-Dimensional Hydraulic Models for River Environments. MSc thesis, Civil, Environmental and Architectural Engineering Department. University of Kansas, USA
16. AlQasimi E, Mahdi T (2018). Unsteady Model for the Hydraulics of Sediments in Rivers. 26th Annual Conference of the ComputationalFluid Dynamics Society of Canada. June 10-12, Winnipeg, MB, Canada
17. AlQasimi E, Pelletier P, Mahdi T (2019b). Flooding of the Saguenay region in 1996: Part 2-Aux Sables River flood mitigation and environmental impact assessment. Natural Hazards. Vol. 96(1):17-32.

18. AlQasimi E, Mahdi T (2019a). Flooding of the Saguenay region in 1996: Part 1-Modeling a flooding in River Ha! Ha!. Natural Hazards. Vol. 96(1):1-15
19. Han Q (1980). A study on the non-equilibrium transportation of suspended load. Proc. of the Int. Symp. on River Sedimentation, Beijing, China, pp. 793-802
20. Jain S C (2000). Open channel flow. Wiley, Chichester
21. Chaudhry MH (2008). Open-Channel Flow. 2nd Ed. Springer Berlin
22. Greimann B, Lai L, Huang JV (2008). Two-Dimensional Total Sediment Load Model Equations. J.Hydraulic Enigneering, ASCE, Vol. 134(8), 1142-1146
23. Parker G (1990). Surface based bedload transport relationship for gravel rivers. Journal of Hydraulic Research 28(4), 417-436
24. Fischer BH (1975) Discussion of 'simple method for predicting dispersion in streams' by R. S. McQuivey and T. N. Keefer. J. Environmental Engineering Division, ASCE 101(3):453-455
25. Armanini, A, Di Silvio G (1988). A One-Dimensional Model for the Transport of a Sediment Mixture in Non-Equilibrium Conditions. J. Hydraulic Research, 26(3):275-292
26. Wu W (2004). Depth-averaged 2-D numerical modeling of unsteady flow and nonuniform sediment transport in open channels. J. Hydraulic Eng., ASCE, 130(10), 1013–1024
27. Meyer-Peter E, Müller R (1948). Formula for bed-load transport. 2nd IAHR Congress Stockholm, 39-64
28. Wong M, Parker G (2006). Reanalysis and Correction of Bed Load Relation of Meyer-Peter and Muller Using Their Own Database. J. Hydraulic Engineering, ASCE, Vol. 132(11). p.1159-1168.
29. Laursen E (1958). The total sediment load of streams. J. Hydraulics Division ASCE 84(HY1):1-36
30. Madden E (1993). Modified Laursen method for estimating bed-material sediment load. USACE-WES. Contract Report HL-93-3
31. Toffaleti F (1968). Definitive computations of sand discharge in rivers. J. Hydraulics Division ASCE 95(HY1):225-246
32. Engelund F, Hansen E (1972). A monograph on sediment transport in alluvial streams. Teknish Forlag, Technical Press, Copenhagen, Denmark
33. Ackers P, White W (1973). Sediment transport: new approach and analysis. J. Hydraulics Division ASCE, 99(HY11):2041-2060
34. HR Wallingford (1990). Sediment transport, the Ackers and White theory revised. Report SR237 HR Wallingford, England

35. Yang CT (1973). Incipient motion and sediment transport. J. Hydraulics Division ASCE 99(HY10):1679-1704
36. Yang CT (1984). Unit stream power equation for gravel. J. Hydraulics Division ASCE 110(HY12):1783-1797
37. Yang CT (1979). Unit stream power equations for total load. J. Hydrology 40: 123-138
38. Yang CT, Molinas A, Wu B (1996). Sediment transport in the Yellow River. Journal of Hydraulic Engineering 122(5): 237-244
39. Wu W (2007). Computational River Dynamics, Taylor & Francis, UK, 494 p
40. Rahuel JL, Holly FM, Chollet JP, Belleudy PJ, Yang G (1989). Modelling of Riverbed Evolution for Bedload sediment Mixtures. Journal of Hydraulic Engineering 115(11), 1521-1542
41. Wu W (1991). The study and application of 1-D, horizontal 2-D and their nesting mathematical models for sediment transport. PhD diss. Wuhan, China: Wuhan University of Hydraulic and Electrical Engineering
42. Krone RB (1962). Flume studies of the transport of sediment in estuarine shoaling processes. Final Report, Hydraulic Engineering Laboratory, University of California, Berkeley
43. Partheniades E (1965). Erosion and deposition of cohesive soils. J. Hydraulics Division. ASCE, 91(HY1):105-139
44. Ariathurai R, Krone RB (1976). Finite element model for cohesive sediment transport. J.Hydraulics Division, ASCE, 102(HY3): 323-338
45. Yang CT, Simoes FJM (2000). User's Manual for GSTARS 2.1 (Generalized Stream tube Model for Alluvial River Simulation Version 2.1). Technical Report. Bureau Reclamation, Technical Service Center. Denver, CO
46. U.S. Interagency Committee on Water Resources, Subcommittee on Sedimentation (1957). Some fundamentals of particle size analysis. Report no. 12
47. Bennet J, Nordin C (1977). Simulation of sediment transport and armoring. Hydrological Sciences Bulletin 22:555-569
48. Yang CT (1972). Unit stream power and sediment transport. ASCE, J. Hydraulics Division, 98(HY 10):1805-1826
49. Chang HC (1988). Fluvial Processes in River Engineering. John Wiley & Sons
50. Henderson FM (1966). Open channel flow. MacMillan Book Company, NY
51. Kutija V, Newett CJM (2002). Modelling of supercritical flow conditions revisited; NewC Scheme. J. Hydraulic Research, 40(2):145-152

52. Yanenko N. N. [1971] The method of fractional steps. The solution of problems of mathematical physics in several variables. Springer-Verlag, NY. 160 p

53. Godunov SK, Riabenkii VS (1987). Difference schemes: an introduction to the underlying theory. English translation by EM Gelbard. North-Holland, NY

54. Cunge JA, Holly FM, Verwey A (1980). Practical aspects of computational river hydraulics. Pitman, London

55. Hirsh C (1990). Numerical computation of internal and external flows: fundamentals of numerical discretization. John Wiley, NY

56. Pletcher RH, Tannehill JC, Anderson DA (2012). Computational Fluid Mechanics and Heat Transfer. 3rd Ed., CRC Press, Boca Raton, FL

57. Versteeg, H., and W. Malalasekera (2007). An Introduction to Computational Fluid Dynamics: The Finite Volume Method. 2nd ed. Prentice Hall.

58. Van Leer B (1974). Towards the ultimate conservative difference scheme. II. Monotonicity and conservation combined in a second-order scheme. J. Computational Physics, 14(4), 361–370

59. Chapra SC, Canale RP (2020). Numerical Methods for Engineers. 8th edition. WCB/McGraw-Hill, NY

60. Cantelli A, Paola C, Parker G (2004). Experiments on upstream-migrating erosional narrowing and widening of an incisional channel caused by dam removal, Water Resources Research, Vol. 40, W03304, doi:10.1029/2003WR002940

List of Tables

Table 1 - Sensitivity analyses' input data sets

Figures' captions

Fig 1 Flowchart of UMHYSER-1D

Fig 2 Schematic representation of stream tubes [2]

Fig 3 Input data illustration for cohesive settling velocity

Fig 4 Simplified diagram for the bed sorting and armoring processes, adapted from [46]. $Qs_{i,k}$: flow carrying capacity for size class *k* during time step *i*, $|\Delta Z_k|$: amount of material in size class *k* eroded during time step *i*, and $|T_{i,k}|$: amount of material of size class *k* present in the active layer, i.e., available for erosion, during time step *i*

Fig 5 Discretization grid of NewC numerical scheme

Fig 6 Discretization grid for convection-diffusion equation

Fig 7 Sensitivity analysis: Effects of sediment transport capacity equation on longitudinal profile evolution

Fig 8 Sensitivity analysis: Effects of angles of repose on longitudinal profile evolution

Fig 9 Sensitivity analysis: Effects of erosional width on longitudinal profile evolution

Fig 10 Sensitivity analysis: Effects of non-dimensional critical shear stress on longitudinal profile evolution

Fig 11 Sensitivity analysis: Effects of the minimization theories on longitudinal profile evolution

Fig 12 Sensitivity analysis: Effects of non-equilibrium coefficients for deposition and erosion on longitudinal profile evolution

Fig 13 Sensitivity analysis: Effects of the diffusive wave approximation on longitudinal profile evolution

Fig 14 Sensitivity analysis: Effects of Manning coefficient on longitudinal profile evolution

Fig 15 Simulated and observed Longitudinal profiles' comparison between Run 6 of [59] and UMHYSER-1D optimum input data set

Fig 16 Example of transverse changes: cross-section corresponding to the knickpoint (Sim 21).

Table 1 - Sensitivity analyses' input data sets

Simulation	Flow Routing	Sediment Equation	θc[1]	Angle of repose (°) Above water	Angle of repose (°) Bellow water	Wer[2] (cm)	L_b[3] (cm)	Minimization	Manning
Base run	Dynamic	Parker[4]	0.0386	70	45	24	10	-	0.025
Sim 1	Dynamic	MPM[5]	-	70	45	24	10	-	0.025
Sim 2	Diffusive	Parker	0.0386	70	45	24	10	-	0.025
Sim 3	Dynamic	MPM-WP[6]	-	70	45	24	10	-	0.025
Sim 4	Dynamic	Parker-SSC[7]	0.0386	70	45	24	10	-	0.025
Sim 5	Dynamic	Parker	0.03	70	45	24	10	-	0.025
Sim 6	Dynamic	Parker	0.045	70	45	24	10	-	0.025
Sim 7	Dynamic	Parker	0.0386	70	40	24	10	-	0.025
Sim 8	Dynamic	Parker	0.0386	70	30	24	10	-	0.025
Sim 9	Dynamic	Parker	0.0386	70	20	24	10	-	0.025
Sim 10	Dynamic	Parker	0.0386	40	40	24	10	-	0.025
Sim 11	Dynamic	Parker	0.0386	70	45	24	00	-	0.025
Sim 12	Dynamic	Parker	0.0386	70	45	24	20	-	0.025
Sim 13	Dynamic	Parker	0.0386	70	45	16	10	-	0.025
Sim 14	Dynamic	Parker	0.0386	70	45	22	10	-	0.025
Sim 15	Dynamic	Parker	0.0386	70	45	20	10	-	0.025
Sim 16	Dynamic	Parker	0.0386	70	45	30	10	-	0.025
Sim 17	Dynamic	Parker	0.0386	70	45	40	10	-	0.025
Sim 18	Dynamic	Parker	0.0386	70	45	24	10	TSP[8]	0.025
Sim 19	Dynamic	Parker	0.0386	70	45	24	10	ES[9]	0.025
Sim 20	Dynamic	Parker	0.0386	70	45	24	10	BS[10]	0.025
Sim 21	Diffusive	Parker	0.045	70	30	30	10	TSP[8]	0.025
Sim 22	Diffusive	Parker	0.045	70	30	30	00	TSP[8]	0.022
Sim 23	Diffusive	Parker	0.045	70	30	30	00	TSP[8]	0.028

1: non-dimensional critical shear stress needed to use Parker's equation [23]; 2: Erosion width; 3: adaptation length for bed load; 4: Meyer Peter and Muller [27]; 5: Parker's equation [23]; 6: Meyer Peter and Muller corrected by Wong and Parker [28]; 7: Parker's equation with shear stress correction [23]; 8: Total Stream Power minimization; 9: Energy Slope minimization; 10: Bed Slope minimization

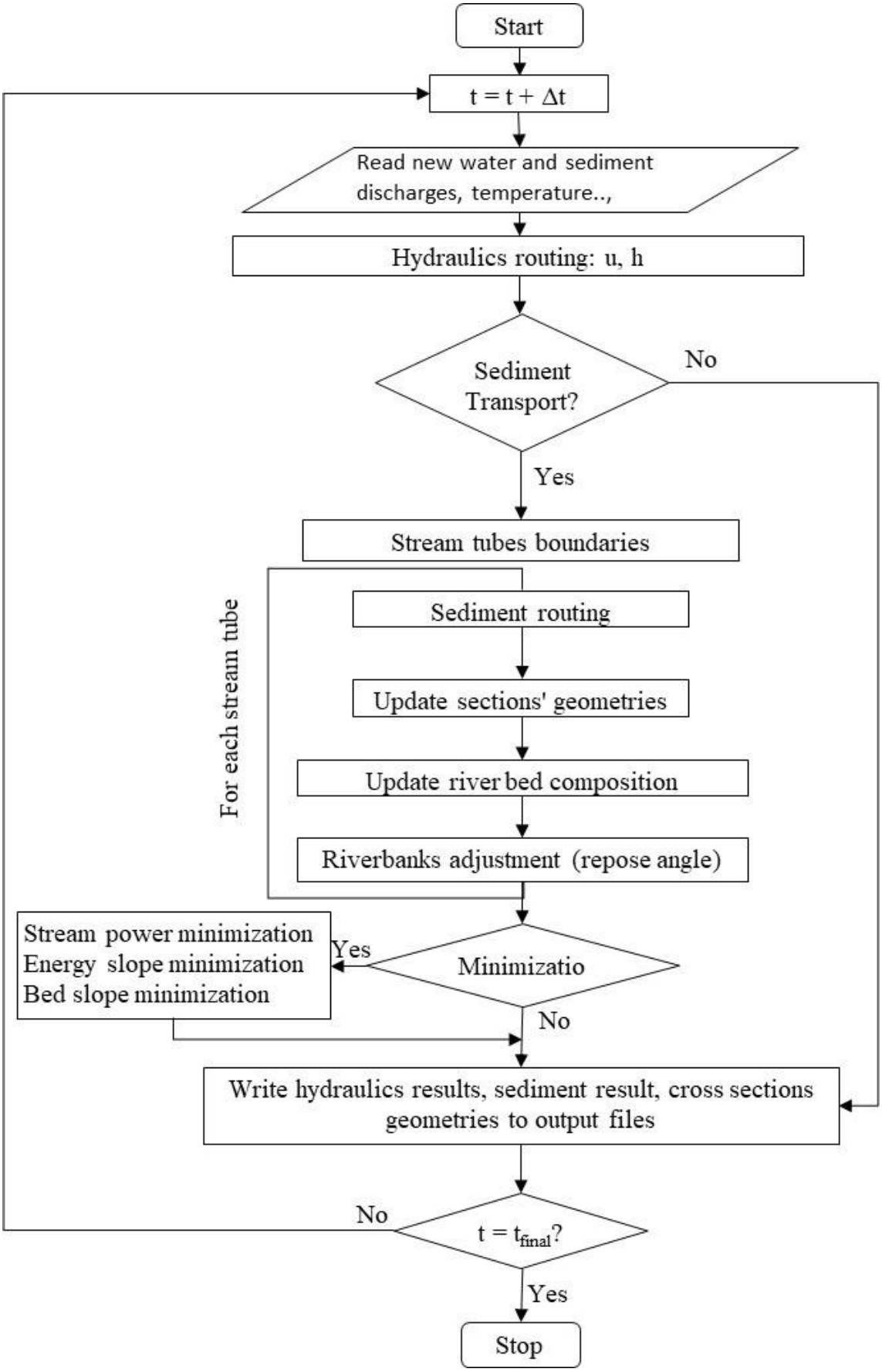

Fig 1 Flowchart of UMHYSER-1D

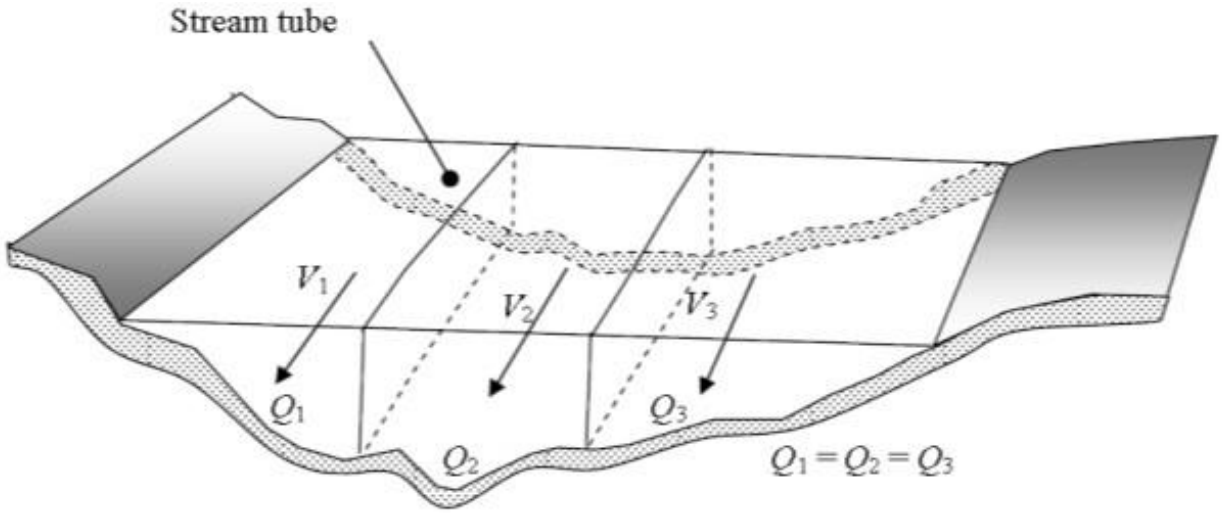

Fig 2 Schematic representation of stream tubes [2]

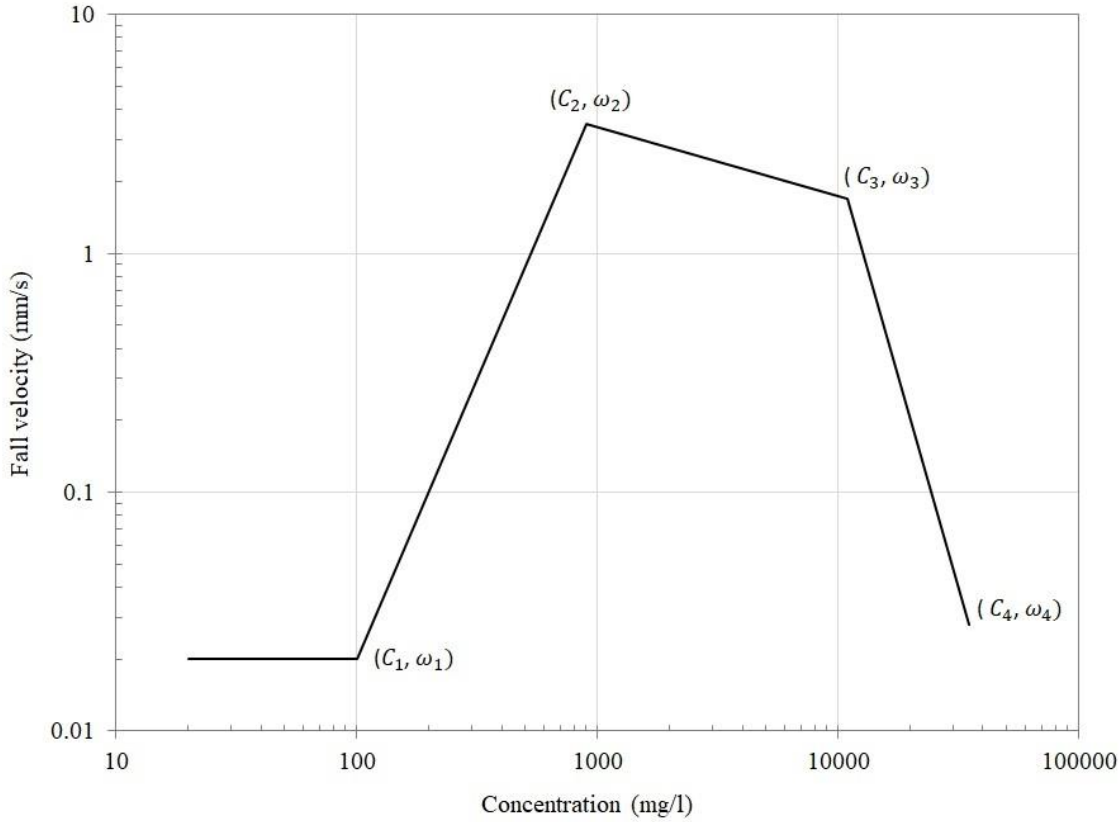

Fig 3 Input data illustration for cohesive settling velocity

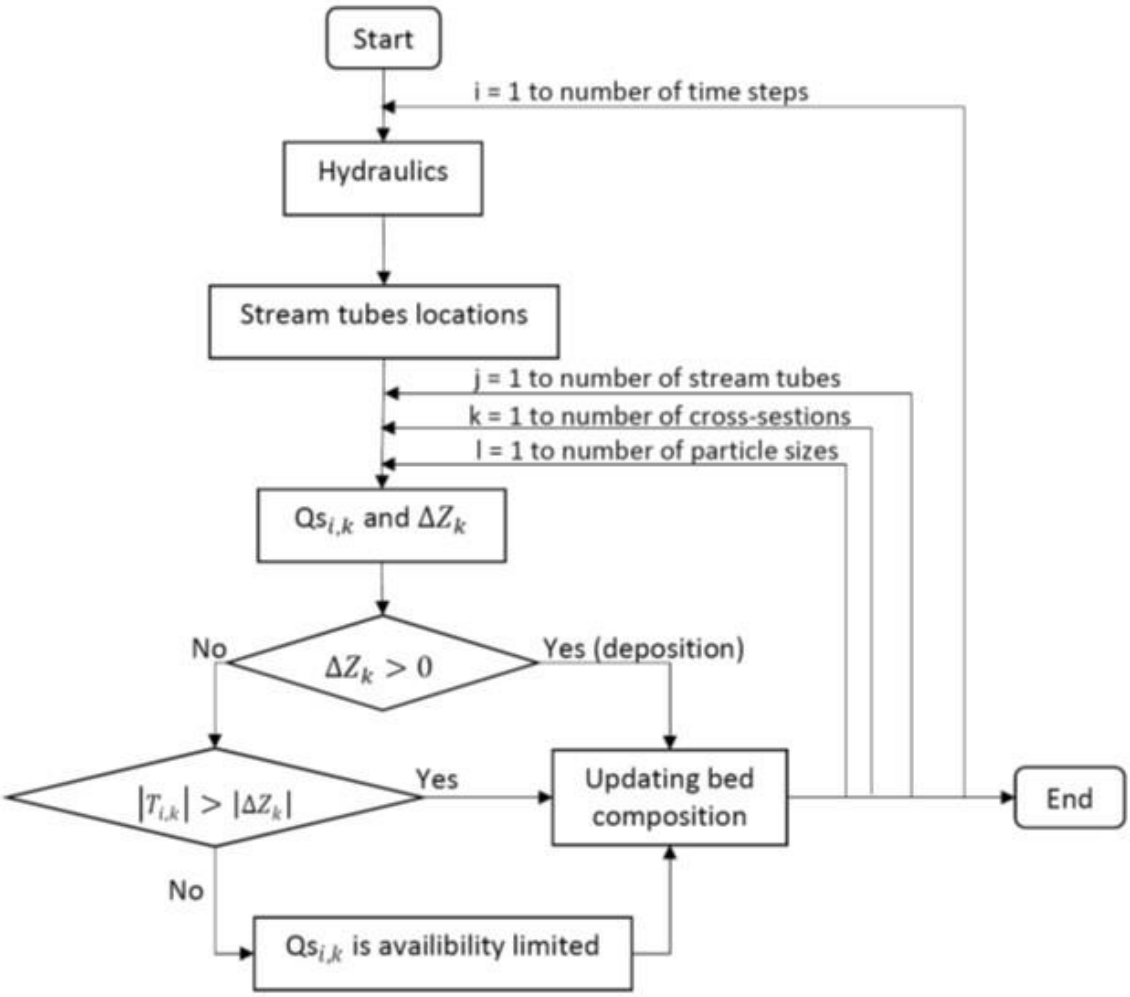

Fig 4 Simplified diagram for the bed sorting and armoring processes, adapted from [46]. $Qs_{i,k}$: flow carrying capacity for size class *k* during time step *i*, $|\Delta Z_k|$: amount of material in size class *k* eroded during time step *i*, and $|T_{i,k}|$: amount of material of size class *k* present in the active layer, i.e., available for erosion, during time step *i*

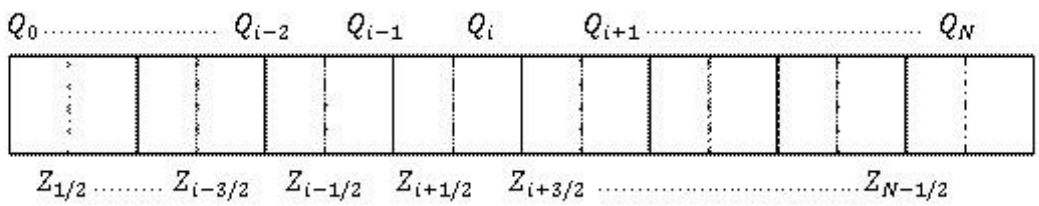

Fig 5 Discretization grid of NewC numerical scheme

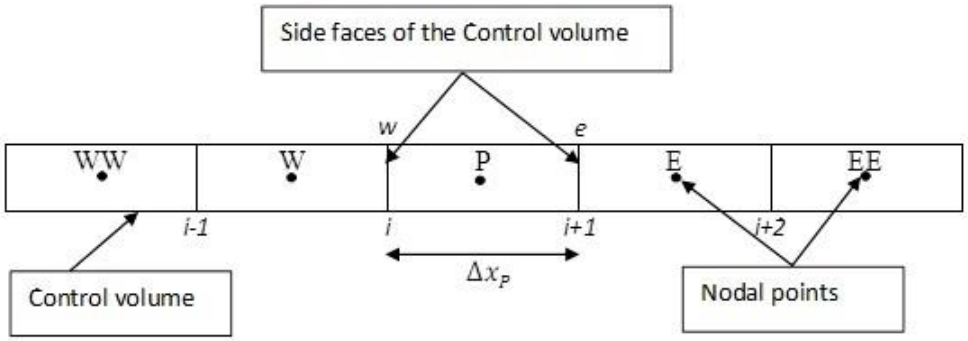

Fig 6 Discretization grid for convection-diffusion equation

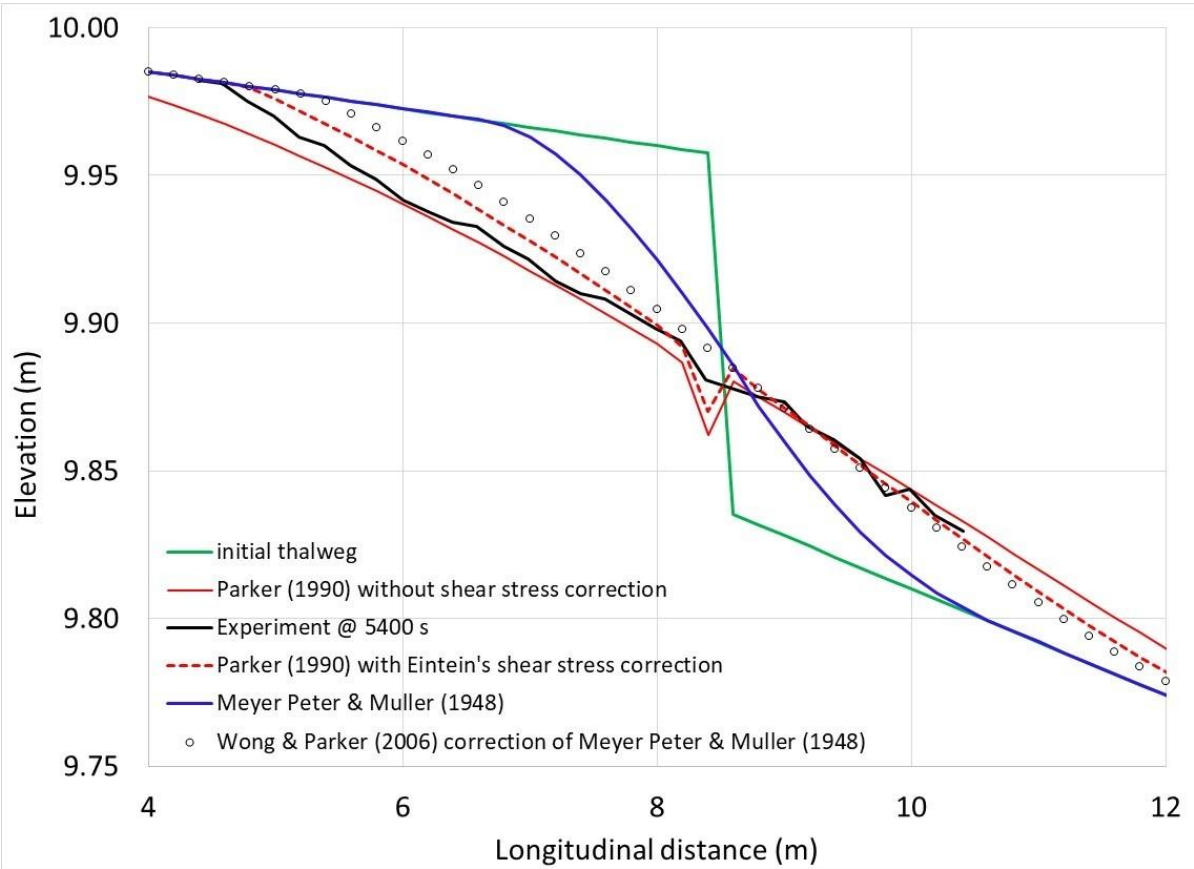

Fig 7 Sensitivity analysis: Effects of sediment transport capacity equation on longitudinal profile evolution

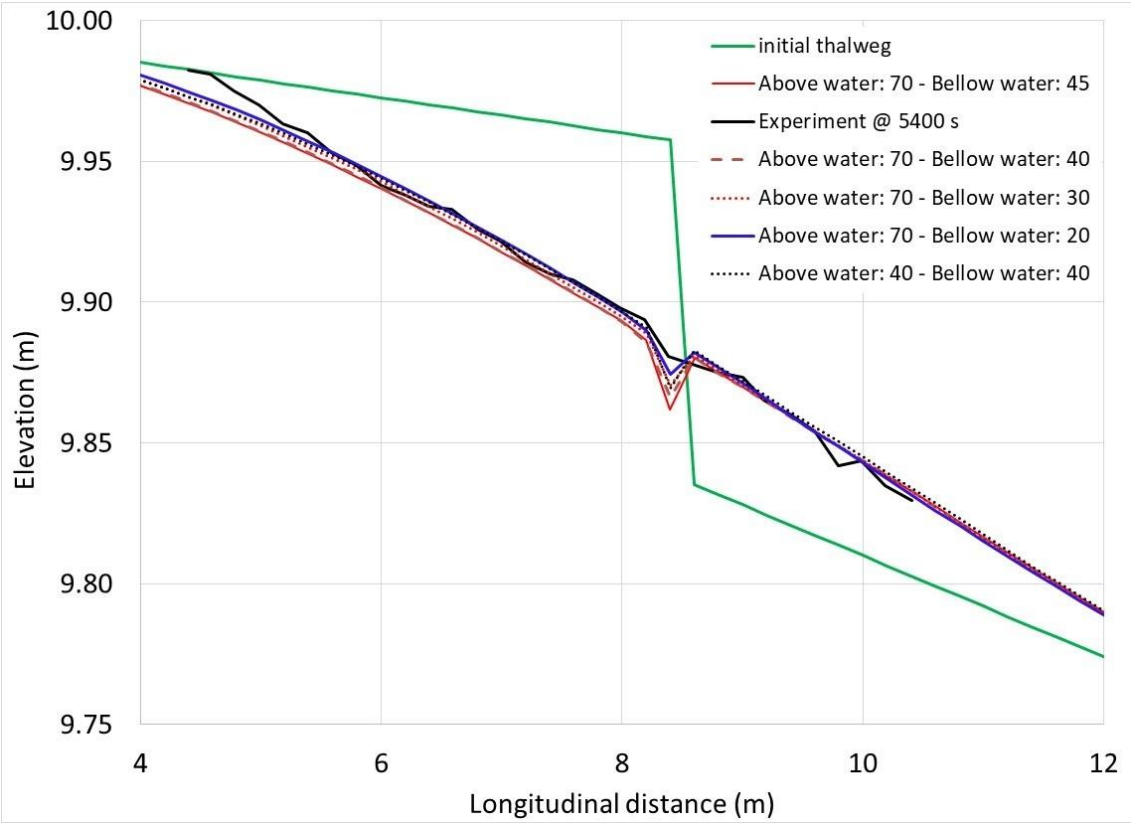

Fig 8 Sensitivity analysis: Effects of angles of repose on longitudinal profile evolution

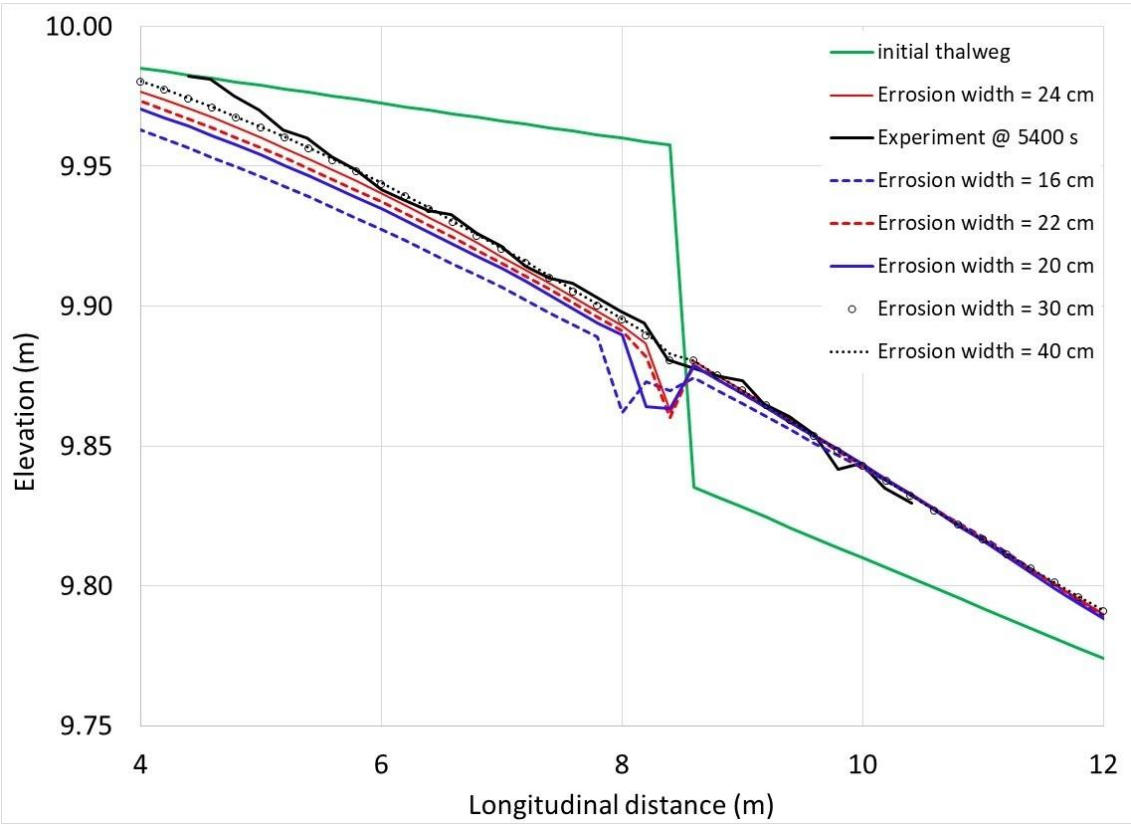

Fig 9 Sensitivity analysis: Effects of erosional width on longitudinal profile evolution

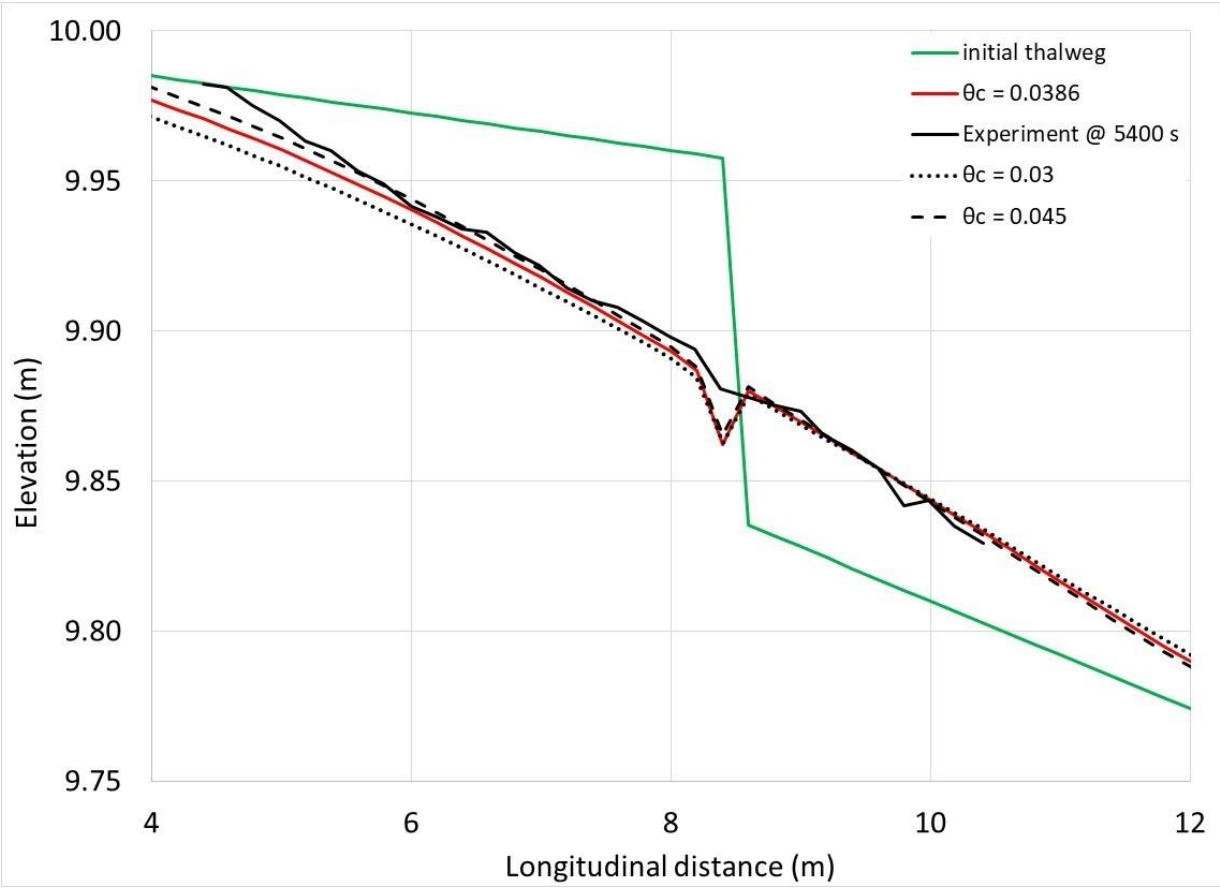

Fig 10 Sensitivity analysis: Effects of non-dimensional critical shear stress on longitudinal profile evolution

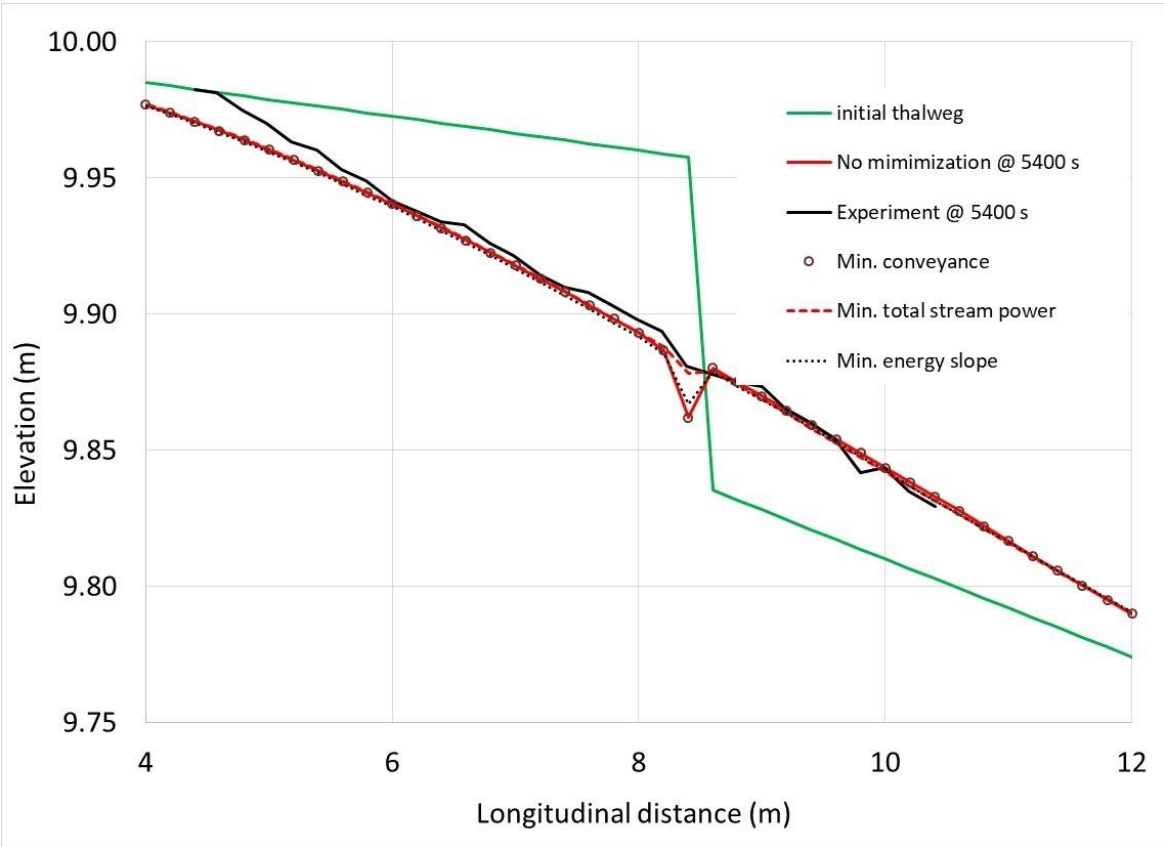

Fig 11 Sensitivity analysis: Effects of the minimization theories on longitudinal profile evolution

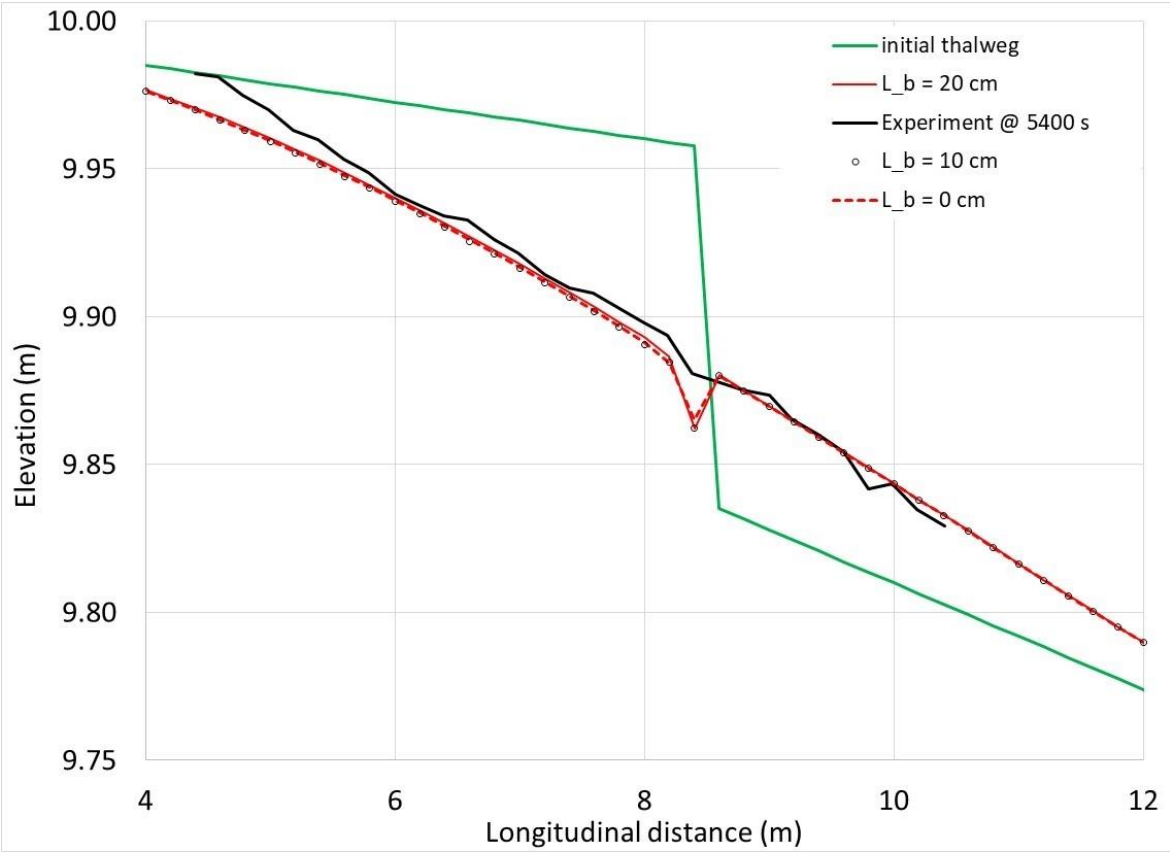

Fig 12 Sensitivity analysis: Effects of non-equilibrium coefficients for deposition and erosion on longitudinal profile evolution

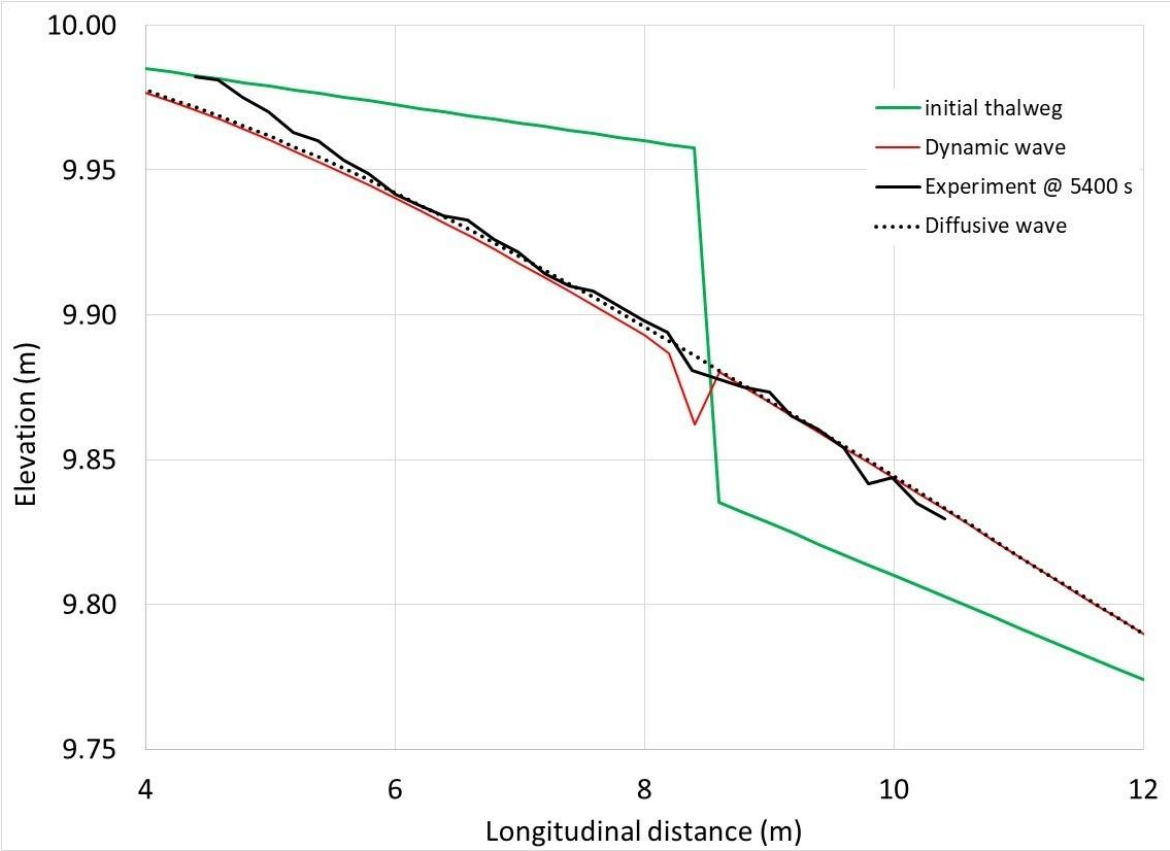

Fig 13 Sensitivity analysis: Effects of the diffusive wave approximation on longitudinal profile evolution

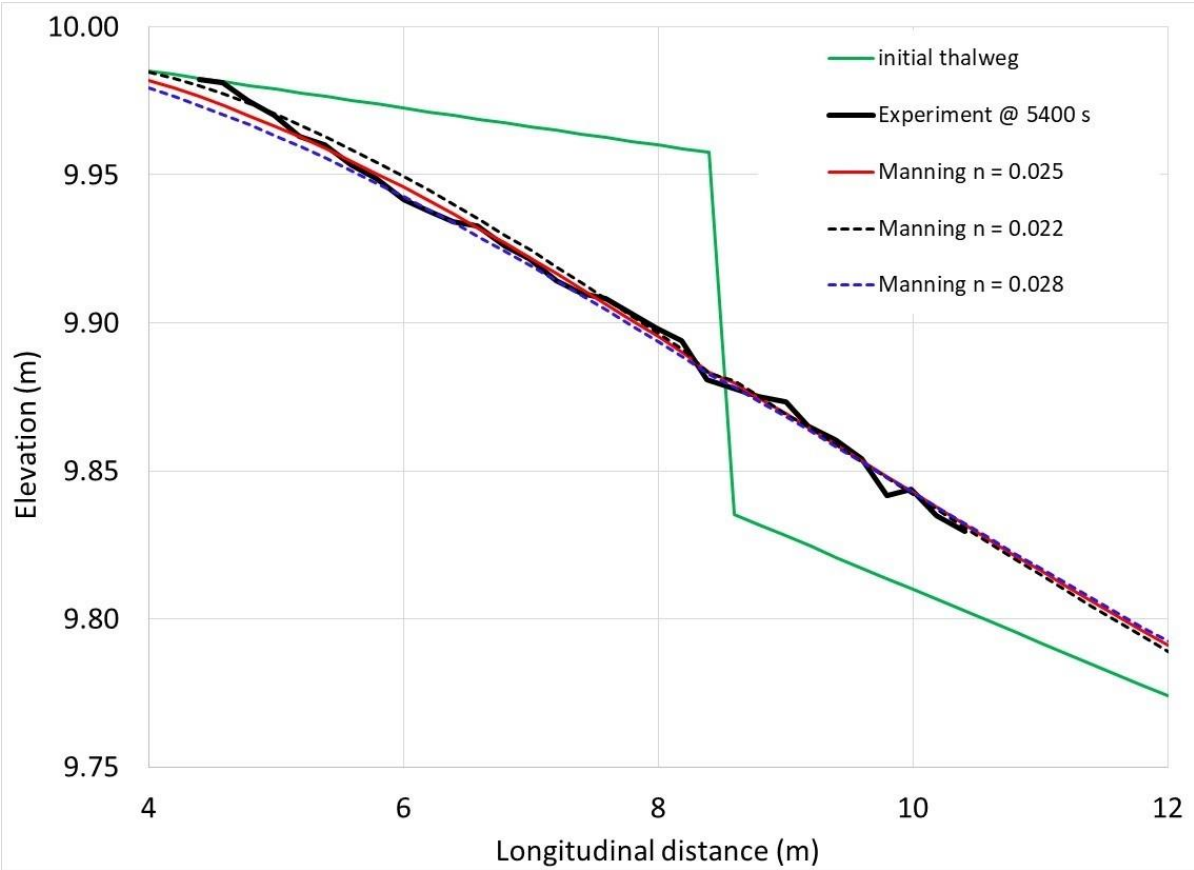

Fig 14 Sensitivity analysis: Effects of Manning coefficient on longitudinal profile evolution

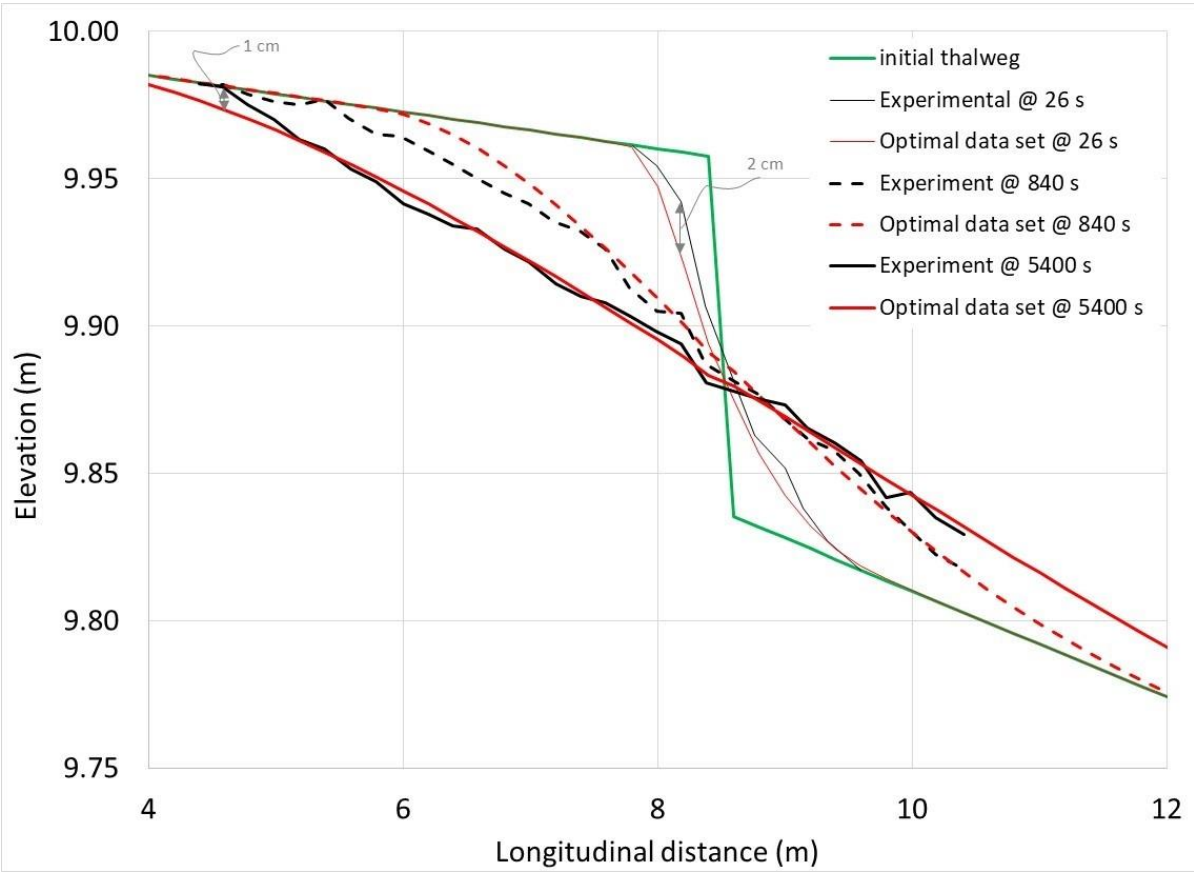

Fig 15 Simulated and observed Longitudinal profiles' comparison between Run 6 of [59] and UMHYSER-1D optimum input data set

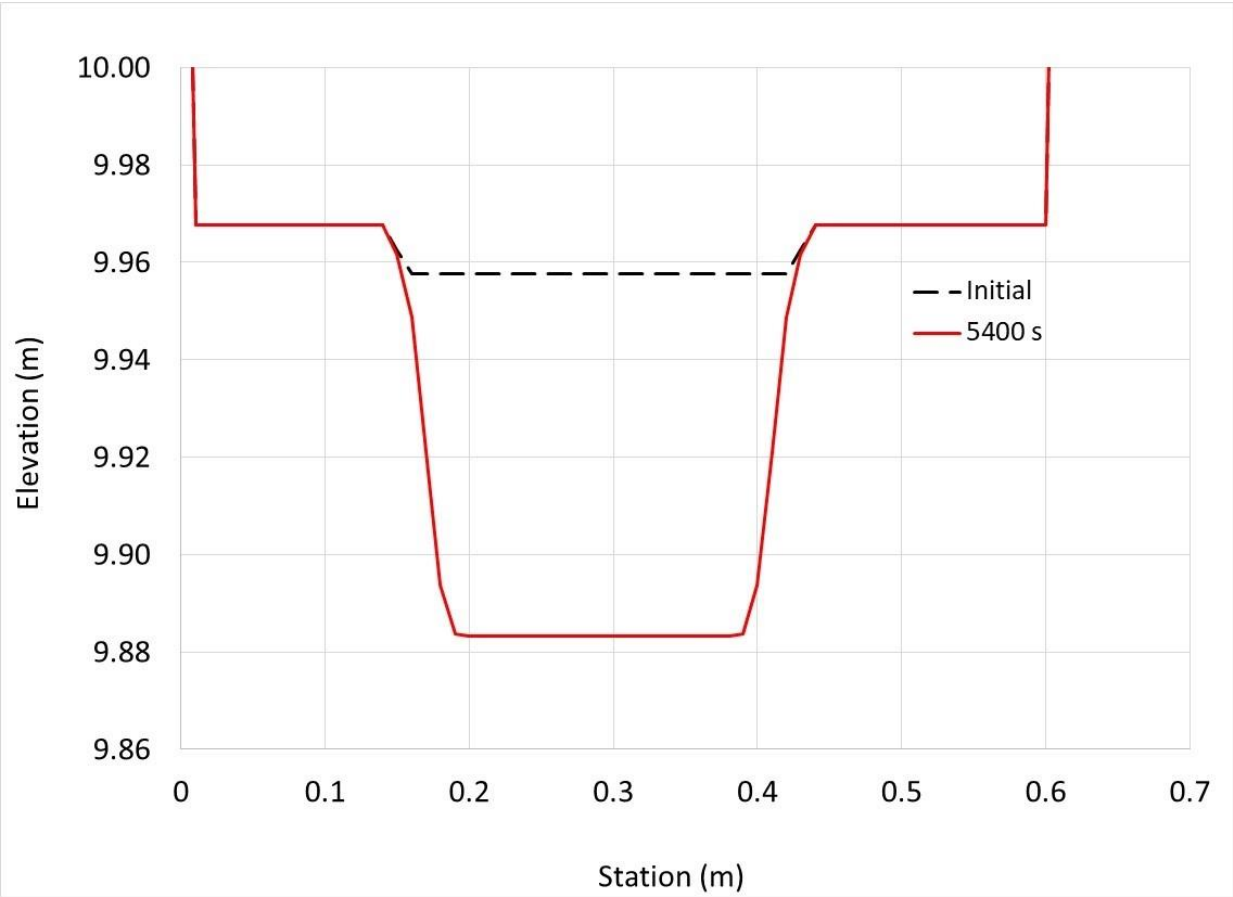

Fig 16 Example of transverse changes: cross-section corresponding to the knickpoint (Sim 21).